Biochimie 214 (2023) 73–82

Contents lists available at ScienceDirect

Biochimie

journal homepage: www.elsevier.com/locate/biochi

Unveiling the structural mechanism of a G-quadruplex pH–Driven switch

Petra Galer [a, 1, 2], Baifan Wang [a, 1, 3], Janez Plavec [a, b, c], Primož Šket [a, *]

[a] Slovenian NMR Center, National Institute of Chemistry, Hajdrihova 19, SI-1000, Ljubljana, Slovenia
[b] EN-FIST Center of Excellence, SI-1000, Ljubljana, Slovenia
[c] Faculty of Chemistry and Chemical Technology, University of Ljubljana, SI-1000, Ljubljana, Slovenia

ARTICLE INFO

Article history:
Received 21 June 2023
Received in revised form
21 July 2023
Accepted 6 August 2023
Available online 10 August 2023

Handling Editor: J.L. Mergny

Keywords:
Base-triple
pH-driven switch
DNA
G-quadruplex
NMR

ABSTRACT

The human telomere oligonucleotide, d[TAGGG(TTAGGG)$_2$TTAGG] (TAGGG), can adopt two distinct 2-G-quartet G-quadruplex structures at pH 7.0 and 5.0, referred to as the TD and KDH$^+$ forms, respectively. By using a combination of NMR and computational techniques, we determined high-resolution structures of both forms, which revealed unique loop architectures, base triples, and base pairs that play a crucial role in the pH-driven structural transformation of *TAGGG*. Our study demonstrated that *TAGGG* represents a reversible pH-driven switch system where the stability and pH-induced structural transformation of the G-quadruplexes are influenced by the terminal residues and base triples. Gaining insight into the factors that regulate the formation of G-quadruplexes and their pH-sensitive structural equilibrium holds great potential for the rational design of novel DNA based pH-driven switches. These advancements in understanding create exciting opportunities for applications in the field of nanotechnology, specifically in the development of bio-nano-motors.

Introduction

Guanine-rich DNA sequences are abundant in the genomes of many organisms and can fold into unique four-stranded structures called G-quadruplexes in the presence of cations. Those sequences have been identified in regions of biological significance, such as human telomeres and oncogene-promoter regions [1–4]. The formation of G-quadruplexes is closely related to various biological processes, including transcription [5,6], replication [7], genome instability [8,9], and diseases such as cancer [10–16]. In addition to their biological importance, G-quadruplexes have also been applied in DNA nanotechnology, DNAzymes, and biosensors due to their unique four-stranded structure and sensitivity to cations and ligand binding [17–25]. For instance, G-quadruplexes can be used to design pH-driven nanodevices, such as nanoswitches, which could have potential applications in various fields, such as biosensors [26].

Two distinct G-quadruplex structures, each consisting of two G-quartet planes, have been observed for human telomere sequences with four GGG repeats (Fig. 1A and B) [27,28]. It has been proposed that the two-quartet G-quadruplex is an intermediate in the folding of the Hybrid-1 and Hybrid-2 G-quadruplex structures observed in human telomeres. Moreover, the two-quartet G-quadruplex has been identified in physiological conditions [29], suggesting its potential biological relevance. The presence of these two-quartet G-quadruplexes underscores the complexity of G-quadruplex folding and highlights the need for further investigation into their potential biological roles.

In our previous study, we investigated the folding of the oligonucleotide d[TAGGG(TTAGGG)$_2$TTAGG] (designated as *TAGGG*), derived from human telomeric DNA, in the presence of KCl. We found that *TAGGG* predominantly adopts two distinct antiparallel basket-type G-quadruplex structures, each consisting of two G-quartets. These structures are referred to as TD and KDH$^+$ forms (Fig. 1C and D) [30]. As previously explained [30], the TD form is thermodynamically controlled, while the protonated KDH$^+$ form is

Abbreviations: CD, circular dichroism; UV, Ultraviolet–visible; DNA, deoxyribonucleic acid; NMR, nuclear magnetic resonance.

* Corresponding author.
E-mail address: primoz.sket@ki.si (P. Šket).

[1] These authors contributed equally to this work.

[2] Present Address: Department of Chemistry, College of Science, Sultan Qaboos University, P.O. Box 36, Postal Code 123, Muscat, Sultanate of Oman.

[3] Present Address: State Key Laboratory of Elemento-Organic Chemistry, Nankai University, 94 Weijin Road, Tianjin, 300071, China.

https://doi.org/10.1016/j.biochi.2023.08.002

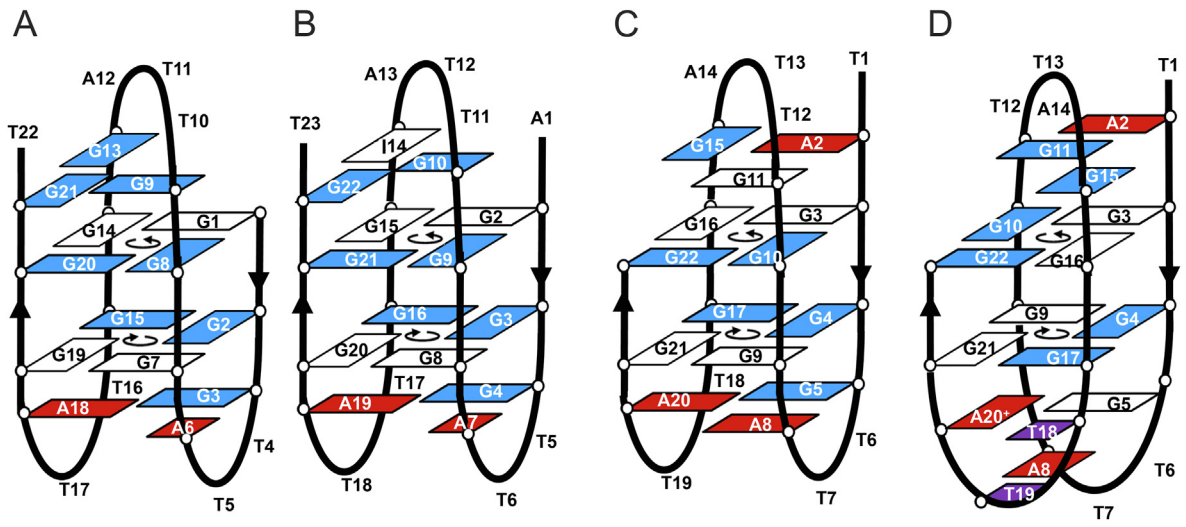

Fig. 1. Topologies of human telomere G-quadruplexes consisting of two G-quartets. **A**) Form 3 G-quadruplex formed by d[(GGGTTA)$_3$GGGT] (PDB ID: 2KF8 [27]), **B**) G-quadruplex formed by d[A(GGGTTA)$_3$GGGT] (PDB ID: 2KKA [28]), **C**) TD form of *TAGGG* (PDB ID: 8JIC), **D**) KDH $^+$ form of *TAGGG* (PDB ID: 8JIH).

kinetically controlled. At pH 7.0, the TD form is dominant and co-exists with a partially pre-folded form of the kinetic G-quadruplex, which we refer to as KD. At lower pH (5.0), the KDH$^+$ form becomes prevalent. The populations of TD, KD, and KDH$^+$ forms are pH-dependent and can be reversibly switched several times, suggesting that *TAGGG* represents a pH-sensitive G-quadruplex pH-driven switch.

In order for a pH-sensitive G-quadruplex system to exhibit effective structural transformations, it is crucial that the structures at both ends of the transformation possess stability while also being capable of facile transformation into another structure. Based on this premise, the present study aimed to investigate the high-resolution structures of the TD and KDH$^+$ forms through comprehensive NMR analysis. The results reveal intriguing loop architectures, unique base triples, and base pairs that play a significant role in maintaining the structural stability of the two G-quartet quadruplexes. We believe that these non-G-quartet structural elements exhibit crucial role in the pH-driven structural transformation. Therefore, the pH-driven structural transformation could potentially be controlled by substituting or deleting residues at the 5′-end and in loop regions. Significant changes are expected already by replacing adenine with thymine residues at the 5′-end and in loop regions, which are involved in the formation of base triples.

2. Materials and methods

2.1. Sample synthesis and preparation

Oligonucleotides without and with partially (8%) ^{15}N,^{13}C site-specifically labeled guanine, adenine, and thymine residues were synthesized on an H-8 synthesizer (K&A Laborgeraete) using standard phosphoramidite solid-phase chemistry following the manufacturer's protocol. Oligonucleotide samples were deprotected with concentrated aqueous ammonia, dialyzed extensively against 2 M LiCl and water, and concentrated using Amicon Ultra-15 centrifugal filter devices. Samples were lyophilized and dissolved in H_2O containing 10% or 100% of ^2H_2O in the presence of 70 mM K^+ ions. pH values were set to 7.0 and 5.0 with the use of 0.5 M HCl and LiOH or potassium phosphate and lithium citrate buffers. Oligonucleotide concentrations used in NMR experiments were between 0.8 and 1.0 mM per strand.

2.2. NMR experiments

All NMR spectra were collected on Agilent Technologies DD2 600 and VNMRS 800 MHz NMR spectrometers at 298 and 278 K using a cold probe. Double pulsed field gradient spin echo (DPFGSE) pulse sequence was used to suppress the water signal. NOESY (nuclear Overhauser effect spectroscopy) spectra were acquired with varying mixing times (τ_m) from 40 to 260 ms in 90% H_2O, 10% ^2H_2O, and 100% ^2H_2O. Double-quantum filtered-COSY, ^{1}H-^{31}P COSY, 1D proton-decoupled ^{31}P NMR spectra and TOCSY (total correlation spectroscopy) spectra with mixing times (τ_m) of 40 and 80 ms were acquired in 100% ^2H_2O. Unambiguous identification of imino, amino, and aromatic protons on 8% ^{15}N,^{13}C site-specifically labeled samples was performed by 1D and 2D^{15}N or ^{13}C-edited HSQC experiments.

Spectra were processed and analyzed using VNMRJ 4.0 (Agilent Technologies) and Sparky (UCSF). NOE (nuclear Overhauser effect) distance restraints for non-exchangeable protons were obtained from a 2D NOESY spectrum recorded in 90% H_2O, 10% ^2H_2O, and 70 mM KCl at pH 7.0, 25 °C for TD and at pH 5.0, 5 °C for KDH$^+$ with varying mixing times (τ_m) from 40 to 260 ms. The average volume of H2''-H1′ cross-peaks of G11, T19, and G17 in TD and of G3, G5, and A14 in KDH$^+$ was used as the distance reference of 1.80 Å. Cross-peaks were classified as strong (1.8–3.6 Å), medium (2.6–5.0 Å), and weak (3.5–6.5 Å).

2.3. NMR structure calculation

The initial extended single-stranded DNA structure was obtained using the leap module of AMBER 14 [31–34]. Structure calculations were performed using the CUDA version of the pmemd module of AMBER 14 program suites [31–34] and parmbsc0 [35] version of the Cornell et al. force field [36] with the 2012 parmχOL4 and 2013 parmε/ζOL1 modification [37,38]. A total of 100 structures were calculated in 80 ps of NMR-restrained simulated annealing (SA) simulations using the generalized Born implicit model. The cut-off for non-bonded interactions was 999 Å and the SHAKE algorithm for hydrogen atoms was used with the 0.4 fs time steps. For each SA simulation, a random velocity was used. The SA simulation was as follows: in 0–2 ps, the temperature was raised from 300 K to 1000 K and held constant at 1000 K for 38 ps. Temperature was scaled down to 500 K in the next 24 ps and reduced to 100 K in the

next 8 ps and was further reduced to 0 K in the last 8 ps. Restraints used in the calculation were NOE-derived distance restraints (force constant 20 kcal mol^{-1} $Å^{-2}$), hydrogen bond (force constant 40 kcal mol^{-1} $Å^{-2}$), torsion angle χ, ε and sugar pucker phase angle restraints (force constant 200 kcal mol^{-1} rad^{-2}). Based on the intensity of respective H8-H1′ 2D NOESY cross-peaks, glycosidic torsion angle for residues G3, G9, G11, G16, and G21 of TD and G3, G5, G9, G16, and G21 of KDH^+ were restrained to the *syn* region (30°–90°). NOE-derived distance restraints were used after the first 3000 steps. All structures were minimized with a maximum of 10 000 steps of energy minimization and a family of 10 structures was selected based on the smallest restraints violations and lowest energy.

The coordinates for TD and KDH $^+$ forms of *TAGGG* have been deposited in the Protein Data Bank (accession codes for TD and KDH^+ are 8JIC and 8JIH, respectively) and BMRB database with accession codes 34034 and 34035 for TD and KDH^+, respectively.

2.4. CD spectroscopy

Circular dichroism (CD) spectra were recorded on an Applied Photophysics Chirascan CD spectrometer at 298 K using a 0.1 cm path-length quartz cell. The wavelength was varied from 200 to 320 nm. Samples for CD measurements were prepared at 20 μM oligonucleotide concentration in 20 mM potassium phosphate buffer (pH 7.0) containing 20 mM KCl or lithium citrate buffer (pH 5.0) with 70 mM K^+ ions.

2.5. UV melting experiments

Thermal stability measurements were performed on a Varian CARY-100 BIO UV-VIS spectrophotometer (Varian Inc.) equipped with a thermoelectric temperature controller. Samples were prepared at 15, 50, 150, and 250 μM oligonucleotide concentrations in 20 mM potassium phosphate buffer (pH 7.0) containing 20 mM KCl. Two cycles of folding/unfolding processes were followed by alternating the temperature between 10 and 90 °C and measuring absorbance at 295 nm using a scanning rate of 0.3 °C min^{-1}.

2.6. Molecular dynamics simulation

A K^+ ion was manually placed in the center of the two G-quartets layers. Then the G-quadruplex was laid in a truncated octahedral box of TIP3P water molecules with the box border at least 10 Å away from any atoms of the G-quadruplex. Extra K^+ ions were added to neutralize the negative charges of the G-quadruplex.

The simulations were performed with the CUDA version of the pmemd module of AMBER 14 [31–34]. Periodic boundary conditions were used, and electrostatic interactions were calculated by the particle mesh Ewald method with the non-bonded cutoff set to 9 Å. The SHAKE algorithm was applied to bonds involving hydrogens, and a 2 fs integration step was used. The pressure was held constant at 1 atm and temperature at 300 K, using the Berendsen weak-coupling thermostat with a relaxation time of 5.0 and Langevin dynamics with a collision frequency of 2.0, respectively.

Before MD simulation, the system was subjected to a series of minimizations and equilibration. The equilibration protocol started with 500 steps of steepest descent minimization followed by 500 steps of conjugate gradient minimization with 25 kcal mol^{-1} A^{-2} position restraints on DNA atoms. Then the system was heated from 0 to 300 K at 100 ps with position restraints of 25 kcal mol^{-1} A^{-2} on G-quadruplex. Afterward, the system underwent minimization with 5 kcal mol^{-1} A^{-2} restraints on DNA atoms using 500 steps of the steepest descent method followed by 500 steps of the conjugate gradient. Continuing in position restraints on DNA atoms of 5 kcal mol^{-1} A^{-2}, the system was equilibrated at 50 ps at a constant temperature of 300 K and pressure of 1 atm. Then an analogous series of alternating minimizations and equilibrations was performed, consecutively using decreasing position restraints of 4, 3, 2, and 1 kcal mol^{-1} A^{-2}. Finally, an equilibration using position restraints of 0.5 kcal mol^{-1} A^{-2} and starting velocities from the previous equilibration, followed by a short 50 ps molecular dynamics took place without any restraints. The productions run for each system last for 100 ns. For the KDH^+ form, the hydrogen bonds between A2 and T12 as well as G11 and G15 were restrained in the first 20 ns. Temperature and pressure coupling used during equilibration was set to 0.2, and coupling during the last molecular dynamics phase was set to 5.

3. Results and discussion

3.1. TAGGG G-quadruplexes with two G-quartet core

In order to obtain high-resolution structures of TD and KDH^+ forms, we first supplement the assignment reported previously [30] by acquiring additional NMR experiments, including 2D ^{13}C-edited HSQC and 2D ^{15}N-edited HSQC spectra to get unambiguous assignment of aromatic and amino proton resonances, respectively as well as 1D proton-decoupled ^{31}P NMR spectra (refer to Figs. S1–S3). Based on previous findings [30], we recorded the spectra for the TD form at pH 7.0 and 298 K, as TD is predominantly formed as the most thermodynamically stable form under these conditions. To determine the high-resolution structure of the KDH^+ form, we obtained spectra at pH 5.0 and 278 K. The lower temperature was deliberately chosen as it exclusively promotes the formation of the kinetically controlled KDH^+ form. The high-resolution structures of the TD and KDH^+ forms were determined by utilizing NOE-derived distance restraints obtained from various regions of the NOESY spectra (refer to Fig. 2, S4, and S5), as well as hydrogen bond and torsion angle restraints (see Table 1).

Fig. 3 depicts the overall structures of the TD and KDH^+ forms, while Figs. S6 and S7 show the families of the ten lowest-energy structures. Both TD and KDH^+ forms have a basket-type topology, consisting of two G-quartets made up of the same guanine residues. The TD and KDH^+ feature one narrow and one wide groove that are separated by two medium grooves. Residues that are part of the wide groove in TD form, are part of the narrow groove in KDH^+, and vice versa (Table 1).

3.2. High-resolution structure of TD form

In the TD form, the segment of G11-G15 is positioned diagonally over the G10→G3→G16→G22 quartet, exhibiting a unique structural architecture where T12, T13, A14, and G15 residues are sequentially stacked with average base tilt angles between T12-T13, T13-A14, A14-G15 of 9 ± 1°, 15 ± 3°, 21 ± 1°, respectively (Fig. 4A). This well-defined structure is characterized by a noticeable chemical shift dispersion of A2P, G11P, T12P, T13P, A14P, and G15P phosphorus signals (from −0.2 to 1.5 ppm, Fig. S3A) and NOEs between these residues (Fig. S4). The G11-G15 segment is stabilized by an A2•G15•G11 base triple, which is positioned over the upper G-quartet with stacking interactions observed among A2 and G16, G15 and G22, as well as G11 and G10 residues (Fig. 3A and S4). The formation of this base triple is supported by NOEs as well as the resonance signals of the imino proton of G15 and amino proton signals of A2 and G15 (Fig. S2A). In the 2D ^{15}N-edited HSQC spectrum at pH 7.0 and 298 K, we also observed an amino proton signal of G11 (Fig. S2A). Although the amino protons of G11 do not participate in hydrogen bonding with other residues, this cross-peak can be explained by molecular dynamics (MD) simulations

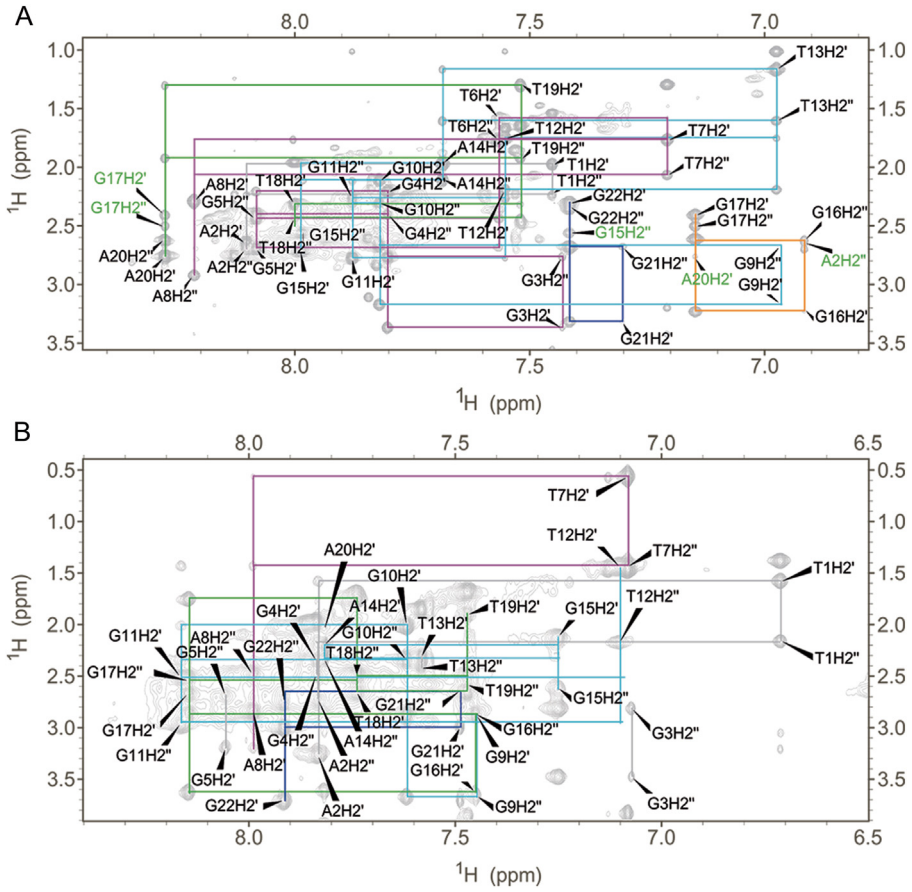

Fig. 2. The H6/H8-H2'/H2" region of the NOESY spectra of **A**) TD and **B**) KDH$^+$ forms. Spectra were acquired in the presence of 70 mM KCl, 10% ^2H_2O and at pH 7.0, 298 K **A**) and at pH 5.0, 278 K **B**). Mixing times were 200 ms in **A**) and 150 ms in **B**). Intraresidual NOE contacts are indicated in black, while green cross-peaks in **A**) represent specific interresidual NOE interactions. Sequential H8/H6- H2'/H2" connectivities for the segments T1-A2, G3-A8, G9-G15, G16-G17, T18-A20 and G21-G22 in TD **A**) and for the segments T1-A2, T7-A8, G9-T12, A14-G15, G16-A20, and G21-G22 in KDH $^+$ **B**) are indicated by solid lines.

Table 1
NMR restraints and structural statistics.

	TD	KDH$^+$
NOE-derived distance restraints		
Intra-residue	186(0)[a]	18(0)
Sequential (i, i + 1)	76(12)	57(7)
Long-range (i, >i + 1)	22(11)	10(36)
Hydrogen bond restraints	20	24
Torsion angle restraints	153	150
Structural statistics		
Mean NOE restraint violation (Å)	0.12 ± 0.03	0.13 ± 0.03
Max. NOE restraint violation (Å)	0.19	0.18
Deviations from idealized geometry		
Bond length (Å)	0.01 ± 0.00	0.01 ± 0.00
Bond angle (°)	2.40 ± 0.03	2.40 ± 0.03
Pairwise heavy atom RMSD (Å)		
Overall	1.42 ± 0.37	1.39 ± 0.31
G-quartet core	0.62 ± 0.13	0.61 ± 0.12
G-quartet core with G11-G15	0.70 ± 0.16	1.21 ± 0.43
G-quartet core with G5-A8	1.03 ± 0.32	0.88 ± 0.20
G-quartet core with T18-A20	0.74 ± 0.17	0.72 ± 0.11
Groove composition and widths (Å)		
Residues G3-T6 and G10-T7	wide, 14.8 ± 0.4	narrow, 4.8 ± 1.2
Residues G16-T18 and G22-T19	narrow, 3.5 ± 1.2	wide, 14.0 ± 0.1
Residues G3-T6 and G16-T18	medium, 7.7 ± 0.6	medium, 5.6 ± 0.5
Residues G10-T7 and G22-T19	medium, 8.1 ± 0.4	medium, 7.4 ± 0.6

[a] Values in parenthesis are from exchangeable protons.

on a 200 ns time scale, which showed that the amino proton of G11 and phosphate group are likely to form a water-mediated hydrogen bond (Fig. S8).

The G17→G4→G9→G21 quartet is capped by an A8•A20•G5 base triple, where A8 and A20 overlap with G21 and G17, respectively, and G5 overlaps with G4. The resonance signals of the amino protons of A8 and A20 support the formation of this triple (Fig. S2A). It is noteworthy that A2, A8, and A20, which are involved in base triples, experience cross-strand stacking interactions rather than being stacked to sequential guanine residues (Fig. 3A and S4).

The T6, T7, T18, and T19 residues, located in two edgewise loops, are either oriented inside the hydrophobic grooves or involved in stacking interactions with each other (Fig. 4B), as observed in the NMR structure ensemble (Figs. S6 and S9A). These interactions are consistent with the hydration properties of the thymine base, as described recently [27]. The T1 residue is the most flexible in the TD structure (Fig. S6).

3.3. High-resolution structure of KDH$^+$ form

KDH$^+$ adopts a unique diagonal loop structure where residue A2 is sandwiched between A14 and a G11•G15 N1-carbonyl base pair (Fig. 4C). A2 is further stabilized by a hydrogen bond between its amino group and the O6 atom of T12 (Fig. 4C). The G11•G15 base pair is stacked on the upper G-quartet, where G11 overlaps with G10, while G15 is positioned between G3 and G16 (Fig. 3B). Although hydrogen bond formation was not observed for the G15 imino proton, its resonance was detected at a chemical shift of

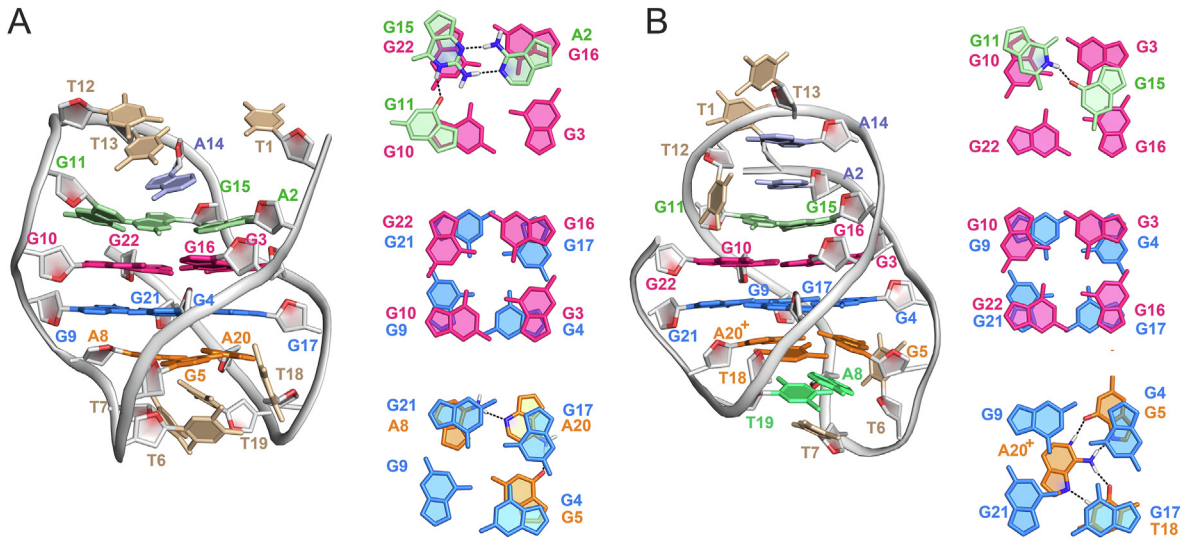

Fig. 3. NMR solution structures of **A**) TD and **B**) KDH$^+$ forms. Stacking interactions between G-quartets and adjacent bases are highlighted on the right side of individual structure, and these interactions are observed from the top to the bottom of the G-quadruplex. Hydrogen, nitrogen, and oxygen atoms involved in hydrogen bonds within base triples and base pairs are colored in grey, blue, and red, respectively. Hydrogen bonds are depicted as dotted lines.

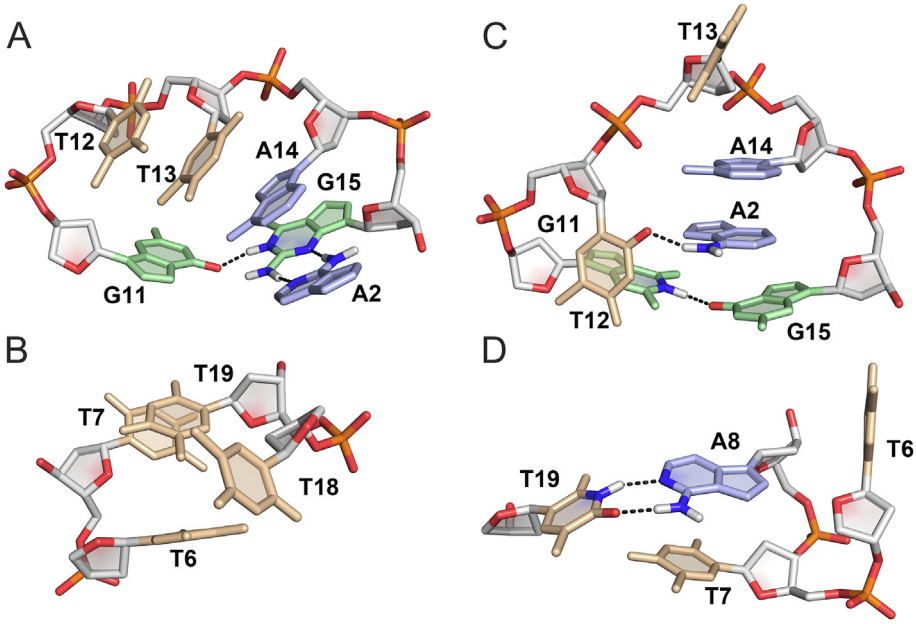

Fig. 4. Comparison of the 'upper' and 'lower' parts of TD (**A** and **B**) and KDH$^+$ (**C** and **D**) forms. **A**) A2•G15•G11 base triple, T12-A14 segment, **B**) thymine residues located in lower part of TD. **C**) A2 residue, G11•G15 base pair, T12-A14 segment and **D**) T19•A8 base pair and orientation of T6, T7 residues in KDH$^+$. Hydrogen, nitrogen, and oxygen atoms involved in hydrogen bonds are colored grey, blue, and red, respectively. Hydrogen bonds are depicted as dotted lines.

δ 8.52 ppm. This proton is located above the center of the upper G-quartet and is tightly packed with A2, G11, and T12, resulting in considerable steric and hydrophobic effects that lower water accessibility and make the G15 imino proton observable in the ^{1}H NMR spectrum (Fig. 4C). This may cause a drastically upfield chemical shift of the G15 imino proton resonance.

The lower G-quartet is stabilized by extensive stacking interactions with a protonated T18•A20$^+$•G5 base triple, which is capped by a T19•A8 Watson-Crick base pair (Figs. 3B and 4D). The imino proton signal for T18 at δ 13.8 ppm and amino proton signals of A20$^+$ at δ 10.7 and 8.5 ppm in the ^{1}H NMR spectra support the formation of the T18•A20$^+$•G5 base triple (Fig. S2B). The A20$^+$ residue is positioned in the center below the bottom G-quartet, while T18 and G5 are stacked on G17 and G4, respectively (Fig. 3B). The observed downfield resonances of G5P (δ 3.1 ppm) and upfield signals of A20$^+$P (δ 1.0 ppm) (Fig. S3B) may be attributed to this unusual base triple and its stacking interaction with the G-quartet. The T19•A8 base pair bridges two edgewise loops across the medium groove and displays stacking between T19 and T18 as well as A8 and G5 residues. The T6 residue is oriented into the narrow groove (Fig. 4D and S9B). T1 and T13 residues are the most flexible parts of the KDH$^+$ (Fig. S7), with the latter showing scarce inter-residue NOE contacts (Fig. S5).

The formation of the G5•A20$^+$•T18 base triple and the stacking mode of the A2 and G11•G15 base pair influence the conformation of the backbone, which is reflected in the ^{31}P NMR spectrum of the

KDH$^+$ form (Fig. S3B). While the majority of the ^{31}P resonances are clustered around δ 0.3 ± 0.8 ppm, there are four phosphorus resonances outside this region. The downfield resonances correspond to G3P (δ 2.7 ppm) and G5P (δ 3.1 ppm), while the upfield signals belong to G11P (δ −0.7 ppm) and A20$^+$P (δ 1.0 ppm).

Base triads and triples [39] are commonly observed in G-quadruplexes [40–43]. To the best of our knowledge, the T18•A20$^+$•G5 base triple in KDH$^+$ is unique, whereas the A2•G15•G11 and A8•A20•G5 base triples in TD (Fig. 3B and S10A, B) exhibit similarities to existing base triads. The A2•G15•G11 base triple can be compared to the G20•(A22-G23) base triad found in the human *MYC* promoter G-quadruplex (Figs. S10A and C). The A8•A20•G5 base triple is reminiscent of the (T1-A2)•A20 triad (Figs. S10B and D) observed in the human telomeric (3 + 1) hybrid-1 G-quadruplex as well as the (T1*-A2*)•A2 triad in the *Bombyx mori* telomeric G-quadruplex [42–44].

3.4. The reversible pH-driven G-quadruplex switch may occur through the formation of a hairpin-like intermediate

We carried out a pH titration experiment to investigate the reversibility of structural changes between TD, KD, and KDH$^+$ forms. To monitor these changes, we integrated the H8/H6 proton signals of the aromatic rings (G16H8 of TD, T1 H6 of KD, and KDH$^+$ forms, see Fig. S11) in ^{1}H NMR spectra. Our findings demonstrate that the pH-induced structural conversion between the three forms is reversible, and this interconversion can occur at least 11 times without any noticeable loss of structural integrity or denaturation (Fig. 5A). During the initial 5 cycles of pH switching, there is a slight increase in the populations of the KDH$^+$ form. As there is 9% of the pre-folded state (determined by fitting of the overlapped signal at δ 8.19 ppm, Fig. S11a), most likely in the form of a hairpin-like structure present at neutral pH besides the TD and KD, continuously repeating the pH switching causes the hairpin-like structure to adopt either TD, KD or at lower pH KDH$^+$ forms. The presence of a pre-folded state was confirmed in the ^{1}H NMR spectra of *TAGGG* in the absence of cations at both pH 5.0 and 7.0. This state was characterized by broad partially overlapped signals of weak intensity around δ 10.8 ppm (Fig. S12). The observed signals in the imino region of the pre-folded state display the typical fingerprint of imino protons from guanine residues involved in GG N1-carbonyl symmetric base pairs [45].

The conversion between TD and KDH$^+$ forms is fast and occurs immediately upon adding aqueous HCl or LiOH into the solution. The timescale of this conversion is similar to the folding process initiated by the addition of K$^+$ ions from a pre-folded hairpin-like structure of *TAGGG*. Rapid conversion between TD and KDH$^+$ could occur by swapping the positions of the first (G3-G5) and fourth (G21-G22) G-tracts, while the second (G9-G11) and third (G15-G17) G-tracts retain their original positions within the G-quadruplex structure (Fig. 5B). Simultaneously, there should be a re-orientation of G11 and G15 residues, which form a GG N1-carbonyl base pair. In TD, G15 acts as the donor of the hydrogen bond, while in KDH$^+$, G11 serves as the donor.

3.5. Influence of 5′ terminal residues on the pH-driven switch

The influence of terminal residues on the stability of G-quadruplex structures has been well-documented [41,43]. To investigate the impact of flanking residues on the pH-driven switch of *TAGGG*, a series of modified sequences were synthesized, including *TTGGG*, *TGGG*, *AGGG*, and *GGG* (abbreviations provided in Table 2).

In the presence of 30 mM KCl at pH 7.0 and 298 K, all four modified sequences at the 5′-end exhibited eight major signals in the imino region of the proton NMR spectra, ranging from δ 10.0–12.5 ppm, indicating the formation of G-quadruplex structures consisting of two G-quartets (Fig. 6A). The modified oligonucleotides displayed slight polymorphic behavior, as indicated by additional smaller signals in the imino regions of the proton spectra. The CD spectra of the modified sequences showed two positive bands at 250 and 295 nm, along with a weak negative band at 264 nm, characteristic of an antiparallel topology (Fig. S13A). The monomolecular nature of modified G-quadruplexes was confirmed by UV melting experiments, which revealed an apparent melting temperature (T_m) independent of concentration. The results showed that substituting A2 with thymine (*TTGGG*) reduced the thermal stability of the G-quadruplex by 4 °C compared to the native sequence (Fig. S14). On the other hand, *TGGG* and *AGGG*

Table 2
TAGGG and its modified sequences.

Abbreviation	Sequence (5′-to-3′)
TAGGG	d(TAGGG TTAGGG TTAGGG TTAGG)
TTGGG	d(TTGGG TTAGGG TTAGGG TTAGG)
TGGG	d(_TGGG TTAGGG TTAGGG TTAGG)
AGGG	d(_AGGG TTAGGG TTAGGG TTAGG)
GGG	d(__GGG TTAGGG TTAGGG TTAGG)
A8T	d(TAGGG TTTGGG TTAGGG TTAGG)
A20T	d(TAGGG TTAGGG TTAGGG TTTGG)

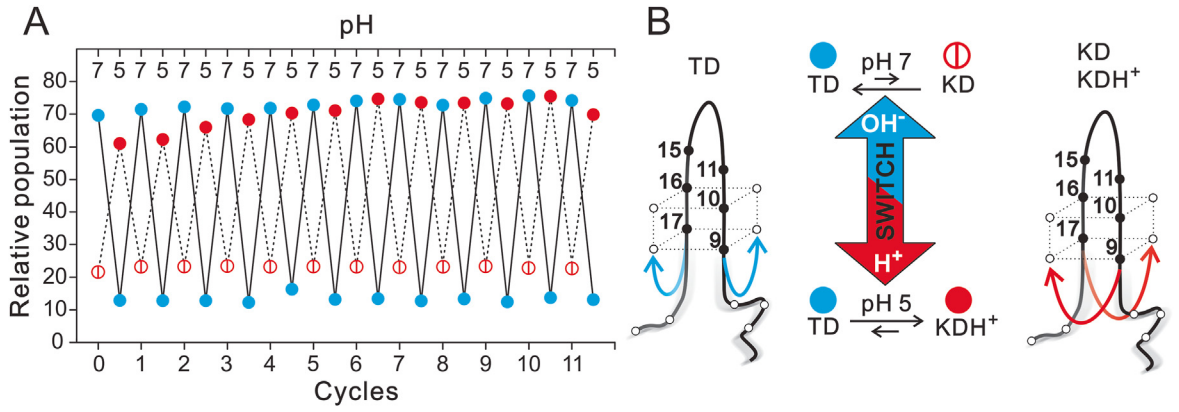

Fig. 5. pH switching experiment performed at 298 K. **A**) Population of TD, KD, and KDH$^+$ forms at two distinct pH values shifted through 11 cycles. pH was adjusted by gradually adding 0.5 M HCl or LiOH solutions into the NMR sample of *TAGGG*. The relative integral (±3 unit %) corresponds to the percentage of TD, KD, and KDH$^+$ forms. An explanation of the symbols corresponding to the TD, KD, and KDH$^+$ forms is provided in panel **B**. **B**) pH shift mechanism is characterized by a preserved mid-transition hairpin-like structure comprised of the G9-G17 segment. Guanine residues within the G9-G17 segment are marked as filled black circles, while empty black circles represent other guanine residues.

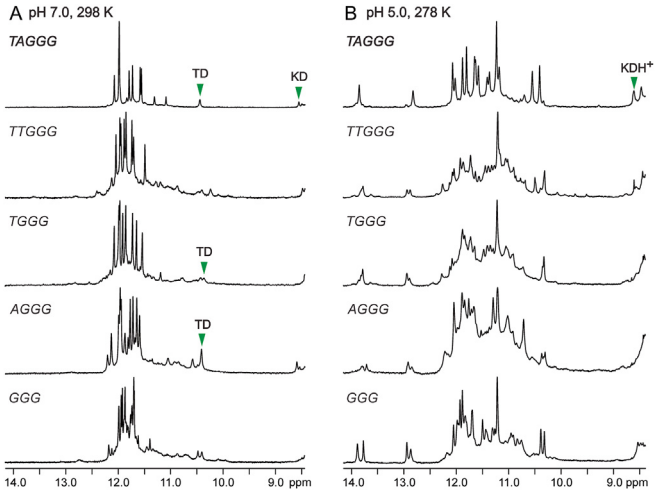

Fig. 6. Imino regions of ^{1}H NMR spectra of parent *TAGGG* and modified oligonucleotides in the presence of 30 mM K^{+} ions. **A**) Spectra obtained at pH 7.0, 298 K. **B**) Spectra obtained at pH 5.0, 278 K. The corresponding oligonucleotide abbreviations are shown on the left side of each spectrum. Green arrows indicate the signals of the G15 imino proton (numbered according to *TAGGG*).

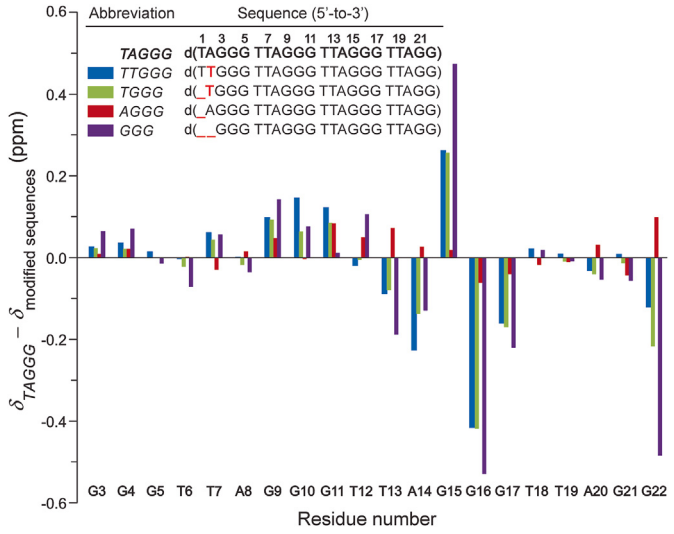

Fig. 7. ^{1}H NMR chemical shift differences for H8/H6 protons between *TAGGG* and its 5′-end modified oligonucleotides. The residues of the modified sequences are numbered according to *TAGGG*.

substitutions increased the T_m values by 4 °C and 7 °C, respectively. Interestingly, GGG exhibited the same T_m value (53 °C) as *AGGG*. These findings indicate that the highly flexible T1 residue decreases the thermal stability of the TD G-quadruplex (T_m for *AGGG* is 7 °C higher than for *TAGGG*), while the formation of A2•G11•G15 base triple increases the stability of the G-quadruplex structure (T_m for *TAGGG* is 4 °C higher than for *TTGGG*).

Although the overall topology of the G-quadruplexes appeared unaffected by the 5′-end modifications, a more detailed structural analysis using partial sequential walks based on the aromatic-H1′ and -H2'/H2" regions of 2D NOESY spectra revealed structural variations in the modified sequences. These variations were primarily observed in certain residues within the diagonal loop and the upper G10→G3→G16→G22 quartet (Figs. S15–S18, for simplicity, the residues in the modified sequences were numbered according to *TAGGG*). Comparative analysis of cross-peak intensities in the aromatic-H1′ region between the modified and parent sequences indicated that the *syn* and *anti*-conformations of the guanine residues within the G-quadruplex core were preserved. However, the orientation around the glycosidic bond of G11 in *TTGGG* and *GGG* was altered. The modifications significantly affected the aromatic proton resonances of G16 and G22, while the H8 proton chemical shifts of the other residues in the upper G-quartet showed minimal changes. The most noticeable differences were observed in the GGG sequence, where the signals of G16H8 and G22H8 exhibited substantial downfield shifts of approximately 0.5 ppm (Fig. 7). Similarly, substantial shifts in the aromatic proton resonance of G16 were observed in the TTGGG and TGGG sequences. In addition to the significant changes in chemical shifts of G16H8 and G22H8, a dramatic shift in the chemical shift of the G15H8 signal was also observed. Notably, the *TTGGG*, *TGGG*, and *GGG* G-quadruplexes, which are unable to form the A2•G15•G11 base triple (Fig. 3A), exhibited upfield chemical shifts of the G15H8 signal. The most significant shift (approximately $\Delta\delta = 0.5$ ppm) was observed in the *GGG* sequence (Fig. 7). In contrast, the *AGGG* sequence showed a negligible shift in the G15 aromatic proton resonance. Similarly, the signal for the G15 imino proton (assigned using partially ^{15}N-labeled oligonucleotides) was observed at a similar chemical shift as in the TD form of the parent sequence for the *AGGG* and *TGGG* G-quadruplexes but was not detected in the *TTGGG* and *GGG* sequences (Fig. 6A). In the AGGG sequence, G15 is most likely involved in the A2•G11•G15 base triple, as indicated by the A2H2"-G16H8 NOE cross-peak, which positions A2 above the upper G-quartet and aligns it closely with G11 and G15 residues from the diagonal loop (Fig. S17). In the TGGG sequence, G15 may participate in the G11•G15 base pair. Furthermore, long-range NOEs between the aromatic protons of A20, G17, and G22, and the H2'/H2" protons of G17, A20, and G15, respectively, which are characteristic of the TD form, were also observed in the NOESY spectra of all four modified sequences (green NOEs in Figs. S15–S18). These cross-strand NOE correlations represent distinctive spectral markers, indicating that G15 is stacked on G22 of the upper quartet and A20 is stacked on G17 of the lower quartet (Fig. 3A). The highly similar NOE patterns, along with characteristic NOE cross-peaks and very similar aromatic proton chemical shifts (Fig. 7), demonstrate that the modified sequences retain the global fold of the TD form with only a few structural differences in parts, which are spatially close to the 5′-end.

To investigate the pH-driven structural transformation of the modified sequences, ^{1}H NMR spectra were obtained at pH 5.0 and 278 K. As we have previously demonstrated, under these conditions, the formation of solely the KDH $^{+}$ form was observed for the *TAGGG* [30]. In the imino regions of the ^{1}H NMR spectra for all four 5′-end modified oligonucleotides, overlapped signals from protons of multiple G-quadruplex structures or even aggregates were observed (Fig. 6b). However, the CD profiles indicated the formation of G-quadruplexes with antiparallel topologies (Fig. S13B). In all ^{1}H NMR spectra, additional signals appeared around δ 13.7 and 12.8 ppm, which were likely attributed to thymine imino protons involved in T18•A20^{+} Hoogsteen and T19•A8 Watson-Crick base pairs, respectively, analogous to the KDH $^{+}$ form of *TAGGG*. The presence of two sets of these signals suggested the coexistence of slightly different G-quadruplexes that maintained the overall structural conformation of KDH^{+}. Among the sequences tested, only *TAGGG* demonstrated complete conversion into the KDH $^{+}$ form, highlighting the significant influence of the T1A2 5′-overhang in stabilizing the entire structure of KDH^{+}.

3.6. Base triples are crucial for the functioning of the pH-driven switch

Base triads and triples play a crucial role in maintaining the structural integrity of G-quadruplexes involved in equilibria [40,43]. To investigate the impact of base triples on the TD, KD, and KDH^+ transformations, we substituted the adenine residues A8 and A20, which are involved in the base triples of the TD and KDH^+ forms, with thymine residues.

At pH 7.0, the replacement of A8 or A20 residue with thymine (A8T and A20T, respectively, as indicated in Table 2) leads to the formation of multiple G-quadruplexes, as evidenced by partially resolved signals in the imino region of the ^{1}H NMR spectra (Fig. 8A). Comparative chemical shift analysis of the G15 imino proton relative to *TAGGG* confirms the presence of TD and KD forms in A8T and A20T sequences. The A8T substitution increases the population of the KD form, as observed from the ratio of integrals for G15 imino proton signals in TD and KD. On the other hand, A20T retains the relative population of TD and KD compared to the parent sequence *TAGGG*. These findings highlight the importance of the A8•A20•G5 base triple for the stability of the TD form.

At pH 5.0 and 278 K, the formation of the KDH^+ form is not observed in the A20T sequence (Fig. 8B). In contrast, A8T adopts the KDH^+ form, as indicated by the intense G15 imino proton signal, while also displaying structural polymorphism based on the presence of overlapping signals. These results indicate that the T18•A20$^+$•G5 base triple is essential for the formation of the KDH^+ form, while the A8 residue contributes to both the stability and polymorphic nature of the KDH^+ form.

3.7. The binding of cations in the loop region of TAGGG G-quadruplexes

The high-resolution crystal structure and MD simulations of the *c-kit* promoter G-quadruplex have indicated the potential importance of non-channel cations in maintaining its structure [46–48]. Our MD simulation results demonstrated that, in addition to the channel ions, K^+ ions can partially stabilize the diagonal loop structures of *TAGGG* G-quadruplexes (Fig. 9). In the TD form, a K^+ ion was observed in the diagonal loop, forming direct contacts with O6 of G11 and G15, OP1 and OP2 of T13, as well as N7 of A14 (Fig. 9A). The occupancy of K^+ ions at this site was approximately 75% during the 20–200 ns simulation period. In the case of the KDH $^+$ form, two binding sites for K^+ ions were identified in the diagonal loop and 5′ terminal of KDH^+ (Fig. 9B). The first binding site, occupied by a K^+ ion at approximately 81%, involved electrostatic interactions between the cation and O4′ and O5′ of A2, OP2 of T13, as well as OP2 and N7 of A14. The second K^+ ion resided between the A2 and G3 residues (i.e., cation ⋯ O4′, O5′, N3 of G3, and O3′ of A2) with 100% occupancy. Considering previous reports on cation-G-quadruplex interactions [46–48], we propose that the binding of cations to the loop region of *TAGGG* G-quadruplexes provides additional stabilization to the loop conformations.

4. Conclusions

In summary, high-resolution structures of TD and KDH^+ forms revealed intriguing loop architectures, unique base triples and base pairs that significantly contributed to structural stabilities of both two G-quartet quadruplexes. Sequence modification studies demonstrate that the most complete conversion into KDH^+ is achieved for *TAGGG* reflecting the importance of both T and A residues at 5′-end as well as A20. Formation of T18•A20$^+$•G5 base triple is essential for existence of KDH^+. A20 residue has thus a crucial role for reaching and regulating a delicate equilibrium between TD, KD and KDH^+. Thus, among all tested sequences only *TAGGG* presents really optimal accessible pH-driven switch system that is perfect in the sense of simple to regulate, quick to response, fine tunable (sensitive to small pH changes) and excellent reversible. It is suggested that the design of DNA based pH system needs to consider the delicate balance between the pH-driven transformation and the stability of the structure in both ends of the structural transformation. The ability to understand and control the structure switching process may allow rational design of DNA pH-driven switches applicable in nanotechnology as bio-nano-motors. Moreover, such structural switching system can be coupled with potential cellular applications based on their different binding affinity and specificities for molecular targets.

Funding

This work was supported by the Slovenian Research Agency (ARRS, grants P1-0242, J1-1704 and J1-7108).

Author contributions

P.G. and P.Š. designed the experiments. P.G. synthesized and prepared DNA oligonucleotide samples and conducted NMR, CD,

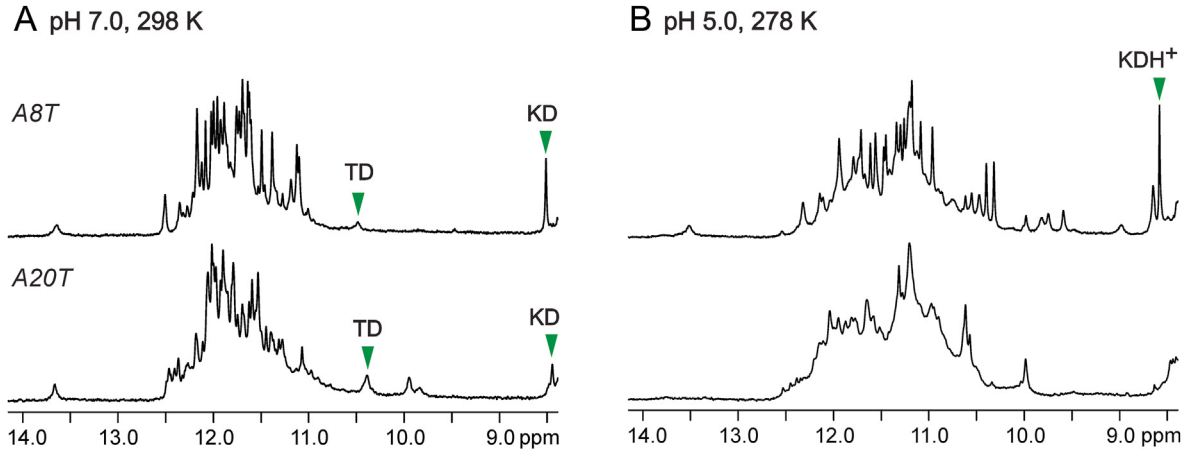

Fig. 8. Imino regions of ^{1}H NMR spectra of A8T and A20T modified oligonucleotides in the presence of 30 mM K^+ ions at **A**) pH 7.0, 298 K, and **B**) pH 5.0, 278 K. Green arrows indicate the signals of G15 imino proton (numbered according to *TAGGG*).

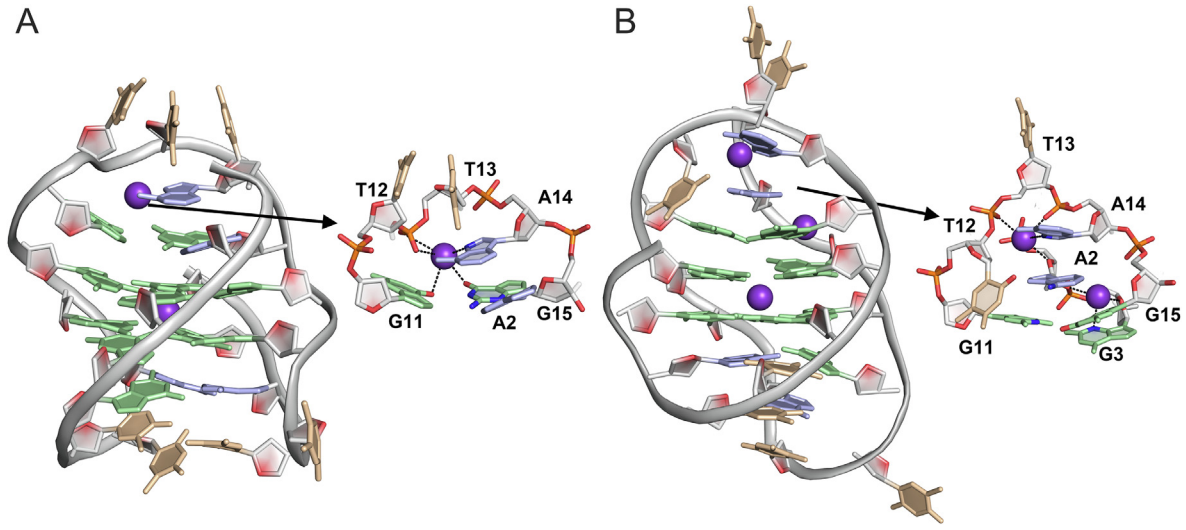

Fig. 9. Potential K^+ ion binding sites of **A**) TD and **B**) KDH^+ forms as suggested by MD simulation. The dashed lines indicate close electrostatic interactions, with a distance below 3.0 Å, between K^+ ions and negatively charged atoms within the loop regions.

and UV experiments. B.W. performed structural calculations and MD simulations. P.G., B.W., J.P., and P.Š. all contributed to analyzing and interpreting the data, as well as writing and revising the manuscript.

Declaration of competing interest

There are no competing interests related to the manuscript:

Appendix A. Supplementary data

Supplementary data to this article can be found online at https://doi.org/10.1016/j.biochi.2023.08.002.

References

[1] V.S. Chambers, G. Marsico, J.M. Boutell, M. Di Antonio, G.P. Smith, S. Balasubramanian, High-throughput sequencing of DNA G-quadruplex structures in the human genome, Nat. Biotechnol. 33 (2015) 877–881, https://doi.org/10.1038/nbt.3295.
[2] A. Bedrat, L. Lacroix, J.L. Mergny, Re-evaluation of G-quadruplex propensity with G4Hunter, Nucleic Acids Res. 44 (2016) 1746–1759, https://doi.org/10.1093/nar/gkw006.
[3] D. Varshney, J. Spiegel, K. Zyner, D. Tannahill, S. Balasubramanian, The regulation and functions of DNA and RNA G-quadruplexes, Nat. Rev. Mol. Cell Biol. 21 (2020) 459–474, https://doi.org/10.1038/s41580-020-0236-x.
[4] I. Frasson, V. Pirota, S.N. Richter, F. Doria, Multimeric G-quadruplexes, A review on their biological roles and targeting, Int. J. Biol. Macromol. 204 (2022) 89–102, https://doi.org/10.1016/j.ijbiomac.2022.01.197.
[5] L.T. Gray, A.C. Vallur, J. Eddy, N. Maizels, G quadruplexes are genomewide targets of transcriptional helicases XPB and XPD, Nat. Chem. Biol. 10 (2014) 313–318, https://doi.org/10.1038/nchembio.1475.
[6] A. Siddiqui-Jain, C.L. Grand, D.J. Bearss, L.H. Hurley, Direct evidence for a G-quadruplex in a promoter region and its targeting with a small molecule to repress *c-MYC* transcription, Proc. Natl. Acad. Sci. USA 99 (2002) 11593–11598, https://doi.org/10.1073/pnas.18225679.
[7] M.L. Bochman, K. Paeschke, V.A. Zakian, DNA secondary structures: stability and function of G-quadruplex structures, Nat. Rev. Genet. 13 (2012) 770–780, https://doi.org/10.1038/nrg3296.
[8] C. Ribeyre, J. Lopes, J.B. Boule, A. Piazza, A. Guedin, V.A. Zakian, J.L. Mergny, A. Nicolas, The yeast Pif1 helicase prevents genomic instability caused by G-quadruplex-forming CEB1 sequences in vivo, PLoS Genet. 5 (2009) e1000475, https://doi.org/10.1371/journal.pgen.1000475.
[9] A. Piazza, M. Adrian, F. Samazan, B. Heddi, F. Hamon, A. Serero, J. Lopes, M.P. Teulade-Fichou, A.T. Phan, A. Nicolas, Short loop length and high thermal stability determine genomic instability induced by G-quadruplex-forming minisatellites, EMBO J. 34 (2015) 1718–1734, https://doi.org/10.15252/embj.201490702.
[10] S.M. Kerwin, G-quadruplex DNA as a target for drug design, Curr. Pharmaceut. Des. 6 (2000) 441–478, https://doi.org/10.2174/1381612003400849.
[11] S. Neidle, Human telomeric G-quadruplex: the current status of telomeric G-quadruplexes as therapeutic targets in human cancer, FEBS J. 277 (2010) 1118–1125, https://doi.org/10.1111/j.1742-4658.2009.07463.x.
[12] S. Balasubramanian, L.H. Hurley, S. Neidle, Targeting G-quadruplexes in gene promoters: a novel anticancer strategy? Nat. Rev. Drug Discov. 10 (2011) 261–275, https://doi.org/10.1038/nrd3428.
[13] A. Bugaut, S. Balasubramanian, 5'-UTR RNA G-quadruplexes: translation regulation and targeting, Nucleic Acids Res. 40 (2012) 4727–4741, https://doi.org/10.1093/nar/gks068.
[14] E.Y.N. Lam, D. Beraldi, D. Tannahill, S. Balasubramanian, G-quadruplex structures are stable and detectable in human genomic DNA, Nat. Commun. 4 (2013) 1796, https://doi.org/10.1038/ncomms2792.
[15] S.A. Ohnmacht, S. Neidle, Small-molecule quadruplex-targeted drug discovery, Bioorg, Med. Chem. Lett. 24 (2014) 2602–2612, https://doi.org/10.1016/j.bmcl.2014.04.029.
[16] B. De Nicola, C.J. Lech, B. Heddi, S. Regmi, I. Frasson, R. Perrone, S.N. Richter, A.T. Phan, Structure and possible function of a G-quadruplex in the long terminal repeat of the proviral HIV-1 genome, Nucleic Acids Res. 44 (2016) 6442–6451, https://doi.org/10.1093/nar/gkw432.
[17] L.A. Yatsunyk, O. Mendoza, J.L. Mergny, "Nano-oddities": unusual nucleic acid assemblies for DNA-based nanostructures and nanodevices, Acc. Chem. Res. 47 (2014) 1836–1844, https://doi.org/10.1021/ar500063x.
[18] J.L. Neo, K. Kamaladasan, M. Uttamchandani, G-quadruplex based probes for visual detection and sensing, Curr. Pharmaceut. Des. 18 (2012) 2048–2057, https://doi.org/10.2174/138161212799958341.
[19] F. Wang, X. Liu, I. Willner, DNA switches: from principles to applications, Angew Chem. Int. Ed. Engl. 54 (2015) 1098–1129, https://doi.org/10.1002/anie.201404652.
[20] D. Pavc, N. Sebastian, L. Spindler, I. Drevensek-Olenik, G.K. Podborsek, J. Plavec, P. Sket, Understanding self-assembly at molecular level enables controlled design of DNA G-wires of different properties, Nat. Commun. 13 (2022) 1062, https://doi.org/10.1038/s41467-022-28726-6.
[21] J.T. Dong, M.P. O'Hagan, I. Willner, Switchable and dynamic G-quadruplexes and their applications, Chem. Soc. Rev. 51 (2022) 7631–7661, https://doi.org/10.1039/d2cs00317a.
[22] J.X. Liu, L. Yan, S.L. He, J.Q. Hu, Engineering DNA quadruplexes in DNA nanostructures for biosensor construction, Nano Res. 15 (2022) 3504–3513, https://doi.org/10.1007/s12274-021-3869-y.
[23] P.K. Lat, C.W. Schultz, H.Z. Yu, D. Sen, A long and reversibly self-assembling 1D DNA nanostructure built from triplex and quadruplex hybrid tiles, Angew. Chem.-Int. Edit. 60 (2021) 8722–8727, https://doi.org/10.1002/anie.202016668.
[24] G. Park, H. Park, S.C. Park, M. Jang, J. Yoon, J.H. Ahn, T.K. Lee, Recent developments in DNA-nanotechnology-powered biosensors for zika/dengue virus molecular diagnostics, Nanomaterials-Basel 13 (2023) 361, https://doi.org/10.3390/nano13020361.
[25] B. Kankia, Quadruplex-based reactions for dynamic DNA nanotechnology, J. Phys. Chem. B 124 (2020) 4263–4269, https://doi.org/10.1021/acs.jpcb.0c02540.
[26] M. Nishio, K. Tsukakoshi, K. Ikebukuro, G.- quadruplex, Flexible conformational changes by cations, pH, crowding and its applications to biosensing, Biosens. Bioelectron. 178 (2021) 113030, https://doi.org/10.1016/j.bios.2021.113030.
[27] K.W. Lim, S. Amrane, S. Bouaziz, W.X. Xu, Y.G. Mu, D.J. Patel, K.N. Luu,

A.T. Phan, Structure of the human telomere in K^+ solution: a stable basket-type G-quadruplex with only two G-tetrad layers, J. Am. Chem. Soc. 131 (2009) 4301–4309, https://doi.org/10.1021/ja807503g.
[28] Z. Zhang, J. Dai, E. Veliath, R.A. Jones, D. Yang, Structure of a two-G-tetrad intramolecular G-quadruplex formed by a variant human telomeric sequence in K^+ solution: insights into the interconversion of human telomeric G-quadruplex structures, Nucleic Acids Res. 38 (2010) 1009–1021, https://doi.org/10.1093/nar/gkp1029.
[29] R. Hansel, F. Lohr, L. Trantirek, V. Dotsch, High-resolution insight into G-overhang architecture, J. Am. Chem. Soc. 135 (2013) 2816–2824, https://doi.org/10.1021/ja312403b.
[30] P. Galer, B. Wang, P. Sket, J. Plavec, Reversible pH switch of two-quartet G-quadruplexes formed by human telomere, Angew Chem. Int. Ed. Engl. 55 (2016) 1993–1997, https://doi.org/10.1002/anie.201507569.
[31] D.A. Case, V. Babin, J.T. Berryman, R.M. Betz, Q. Cai, D.S. Cerutti, T.E. Cheatham, T.A. Darden, R.E. Duke, H. Gohlke, A.W. Gotz, S. Gusarov, N. Homeyer, P. Janowski, J. Kaus, I. Kolossváry, A. Kovalenko, T.S. Lee, S. Le Grand, T. Luchko, R. Luo, B. Madej, K.M. Merz, F. Paesani, D.R. Roe, A. Roitberg, C. Sagui, R. Salomon-Ferrer, G. Seabra, C.L. Simmerling, W. Smith, J. Swails, R.C. Walker, J. Wang, R.M. Wolf, X. Wu, P.A. Kollman, AMBER 14, University of California, San Francisco, 2014.
[32] A.W. Gotz, M.J. Williamson, D. Xu, D. Poole, S. Le Grand, R.C. Walker, Routine microsecond molecular dynamics simulations with AMBER on GPUs. 1. Generalized Born, J. Chem. Theor. Comput. 8 (2012) 1542–1555, https://doi.org/10.1021/ct200909j.
[33] S. Le Grand, A.W. Gotz, R.C. Walker, SPFP: speed without compromise-A mixed precision model for GPU accelerated molecular dynamics simulations, Comput. Phys. Commun. 184 (2013) 374–380, https://doi.org/10.1016/j.cpc.2012.09.022.
[34] R. Salomon-Ferrer, A.W. Gotz, D. Poole, S. Le Grand, R.C. Walker, Routine microsecond molecular dynamics simulations with AMBER on GPUs. 2. Explicit solvent particle mesh Ewald, J. Chem. Theor. Comput. 9 (2013) 3878–3888, https://doi.org/10.1021/ct400314y.
[35] A. Perez, I. Marchan, D. Svozil, J. Sponer, T.E. Cheatham, C.A. Laughton, M. Orozco, Refinenement of the AMBER force field for nucleic acids: improving the description of alpha/gamma conformers, Biophys. J. 92 (2007) 3817–3829, https://doi.org/10.1529/biophysj.106.097782.
[36] W.D. Cornell, P. Cieplak, C.I. Bayly, I.R. Gould, K.M. Merz, D.M. Ferguson, D.C. Spellmeyer, T. Fox, J.W. Caldwell, P.A. Kollman, A second generation force field for the simulation of proteins, nucleic acids, and organic molecules (vol 117, pg 5179, 1995), J. Am. Chem. Soc. 118 (1996) 2309, https://doi.org/10.1021/ja955032e, 2309.
[37] M. Krepl, M. Zgarbova, P. Stadlbauer, M. Otyepka, P. Banas, J. Koca, T.E. Cheatham 3rd, P. Jurecka, J. Sponer, Reference simulations of noncanonical nucleic acids with different chi variants of the AMBER force field: quadruplex DNA, quadruplex RNA and Z-DNA, J. Chem. Theor. Comput. 8 (2012) 2506–2520, https://doi.org/10.1021/ct300275s.
[38] M. Zgarbova, F.J. Luque, J. Sponer, T.E. Cheatham 3rd, M. Otyepka, P. Jurecka, Toward improved description of DNA backbone: revisiting epsilon and zeta torsion force field parameters, J. Chem. Theor. Comput. 9 (2013) 2339–2354, https://doi.org/10.1021/ct400154j.
[39] V.V. Kuryavyi, T.M. Jovin, Triad-DNA: a model for trinucleotide repeats, Nat. Genet. 9 (1995) 339–341, https://doi.org/10.1038/ng0495-339.
[40] A.T. Phan, V. Kuryavyi, K.N. Luu, D.J. Patel, Structure of two intramolecular G-quadruplexes formed by natural human telomere sequences in K^+ solution, Nucleic Acids Res. 35 (2007) 6517–6525, https://doi.org/10.1093/nar/gkm706.
[41] J. Dai, C. Punchihewa, A. Ambrus, D. Chen, R.A. Jones, D. Yang, Structure of the intramolecular human telomeric G-quadruplex in potassium solution: a novel adenine triple formation, Nucleic Acids Res. 35 (2007) 2440–2450, https://doi.org/10.1093/nar/gkm009.
[42] K.N. Luu, A.T. Phan, V. Kuryavyi, L. Lacroix, D.J. Patel, Structure of the human telomere in K^+ solution: an intramolecular (3+1) G-quadruplex scaffold, J. Am. Chem. Soc. 128 (2006) 9963–9970, https://doi.org/10.1021/ja062791w.
[43] J.X. Dai, M. Carver, C. Punchihewa, R.A. Jones, D.Z. Yang, Structure of the Hybrid-2 type intramolecular human telomeric G-quadruplex in K^+ solution: insights into structure polymorphism of the human telomeric sequence, Nucleic Acids Res. 35 (2007) 4927–4940, https://doi.org/10.1093/nar/gkm522.
[44] A. Kettani, S. Bouaziz, W. Wang, R.A. Jones, D.J. Patel, Bombyx mori single repeat telomeric DNA sequence forms a G-quadruplex capped by base triads, Nat. Struct. Biol. 4 (1997) 382–389, https://doi.org/10.1038/nsb0597-382.
[45] S. Ceru, P. Sket, I. Prislan, J. Lah, J. Plavec, A new pathway of DNA g-quadruplex formation, Angew Chem. Int. Ed. Engl. 53 (2014) 4881–4884, https://doi.org/10.1002/anie.201400531.
[46] D. Wei, G.N. Parkinson, A.P. Reszka, S. Neidle, Crystal structure of a *c-kit* promoter quadruplex reveals the structural role of metal ions and water molecules in maintaining loop conformation, Nucleic Acids Res. 40 (2012) 4691–4700, https://doi.org/10.1093/nar/gks023.
[47] B. Islam, P. Stadlbauer, M. Krepl, J. Koca, S. Neidle, S. Haider, J. Sponer, Extended molecular dynamics of a c-kit promoter quadruplex, Nucleic Acids Res. 43 (2015) 8673–8693, https://doi.org/10.1093/nar/gkv785.
[48] D. Wei, J. Husby, S. Neidle, Flexibility and structural conservation in a c-KIT G-quadruplex, Nucleic Acids Res. 43 (2015) 629–644, https://doi.org/10.1093/nar/gku1282.